Journal of Environmental Quality TECHNICAL REPORTS

VADOSE ZONE PROCESSES AND CHEMICAL TRANSPORT

Roots-Enhanced Preferential Flows in Deciduous and Coniferous Forest Soils Revealed by Dual-Tracer Experiments

Ziteng Luo, Jianzhi Niu,* Linus Zhang, Xiongwen Chen, Wei Zhang, Baoyuan Xie, Jie Du, Zhijun Zhu, Shanshan Wu, and Xiang Li

Abstract

Macropores formed by roots are crucial channels for preferential flows in forest soils that are largely responsible for water percolation and solute leaching. Using dual-tracer experiments (Brilliant Blue FCF and bromide [Br^-]), this study investigated the preferential flows of water and solutes in a deciduous forest dominated by *Quercus variabilis* Bl. and a coniferous forest mainly planted with *Platycladus orientalis* (L.) Franco. Dye-stained patterns and concentrations of Brilliant Blue and Br^- were obtained in vertical soil profiles (0–30 cm), whereas stained and unstained roots were collected and analyzed in horizontal soil profiles to a 30-cm soil depth. Brilliant Blue and Br^- were mainly accumulated in the 0- to 20-cm soil depth, which had greater total root length density than the 20- to 30-cm soil depth ($P < 0.05$). Only part of the roots facilitated the preferential flows, with finer roots (i.e., diameter <1 mm) contributing the most. More intriguingly, the coniferous forest soil had a greater degree of preferential flows and greater tracer concentrations at deeper soil depth than the deciduous forest soil, suggesting the importance of tree species and forest composition on water and solute transport in forest ecosystems.

Core Ideas

- Roots enhanced preferential flows, with the primary contribution from finer roots.
- Brilliant Blue and Br^- tracers mainly accumulated in soils with abundant roots.
- Preferential flows were greater in coniferous forest than deciduous forest.

J. Environ. Qual. 48:136–146 (2019)
doi:10.2134/jeq2018.03.0091
Received 4 Mar. 2018.
Accepted 18 Oct. 2018.
*Corresponding author (nexk@bjfu.edu.cn).

Preferential flow is a common process that can control the movement of water and solutes and result in complex flow patterns in the vadose zone (Flury et al., 1994; Wang and Zhang, 2011; Zhang et al., 2011; Nimmo, 2012). Field studies have found that preferential flow may contribute from 11 to 54% of total water flux and carry solutes to bypass a large part of the soil matrix (Stone and Wilson, 2006; Legout et al., 2009; van der Heijden et al., 2013; Laine-Kaulio et al., 2014). Such phenomena can lead to a substantial leaching of nutrients (such as nitrate) and contaminants in soils and thus increase the risk of groundwater pollution (Yasuda et al., 2001; Bachmair et al., 2009).

Although macropores only contribute a small portion to total soil porosity, they play a pivotal role in preferential flow (Wilson and Luxmoore, 1988; Moret and Arrúe, 2007). They are mainly formed by earthworm burrows, root channels, soil shrinkage cracking, chemical weathering, or freezing–thawing cycles and typically have large pore size (>75 μm) and continuity that facilitate the preferential transport of water and solutes (Beven and Germann, 1982; Sheng et al., 2014; Liu and Lennartz, 2015). Both living and decayed roots could serve as preferential flow paths, and root exudates could enhance soil aggregation and subsequently the formation of inter-aggregate macropores (Fageria and Stone, 2006; Ghestem et al., 2011; Vannoppen et al., 2015). In addition, root channels could create well-connected water conduits that are dependent on root system characteristics (Noguchi et al., 1997; Sidle et al., 2001; Newman et al., 2004). For example, root systems with relatively large and shallow roots well connected with plant stems could facilitate lateral subsurface flows, whereas root systems with larger vertical taproots and thinner lateral roots would enhance the vertical water flow (Ghestem et al., 2011). Thus, root system characteristics (e.g.,

Z.T. Luo, J.Z. Niu, B.Y. Xie, J. Du, Z.J. Zhu, S.S. Wu, Key Lab. of Soil and Water Conservation and Desertification Combating of the Ministry of Education, Engineering Research Center of Forestry Ecological Engineering, Ministry of Education, Beijing Forestry Univ., Beijing 100083, China; Z.T. Luo and J.Z. Niu, Beijing Collaborative Innovation Center for Eco-environmental Improvement with Forestry and Fruit Trees, Beijing 102206, China; L. Zhang, Dep. of Water Resources Engineering, Lund Univ., Box 118, 221 00 Lund, Sweden; X.W. Chen, Dep. of Biological and Environmental Sciences, Alabama A&M Univ., Normal, AL 35762; W. Zhang, Dep. of Plant, Soil and Microbial Sciences, Michigan State Univ., East Lansing, MI 48824, USA; X. Li, China National Forestry Economics and Development Research Center, State Forestry Administration, Beijing, 100714, China. Assigned to Associate Editor Hyunjung Kim.

Abbreviations: BB, Brilliant Blue FCF; RLD, root length density; DF, deciduous forest; CF, coniferous forest.

rooting depth and root size) could influence the infiltration rate and redistribution of water in soils (Archer et al., 2002; Leung et al., 2015). Indeed, Devitt and Smith (2002) found that the enhancement of water percolation by root channels increased with increasing size of root systems. Therefore, there are intriguing interplays among plant roots, macropore flows, and solute transport in the vadose zone.

In forest soils, these interrelationships are particularly important as root channels are considered to be primary preferential pathways (Elçi and Molz, 2009; Laine-Kaulio et al., 2015; Zhang et al., 2016). Vegetation species in a forest can be diverse, including shrubs, coniferous and deciduous tree species, and so on (Jia et al., 2017). However, to date, little is known concerning how tree species (each with their unique root systems) may influence preferential flows in forest soils. It is recognized that coniferous trees have well-developed deeper roots at 40- to 60-cm soil depth, whereas deciduous trees have well-developed roots in shallow soils (0–25 cm) (Bauhus and Messier, 1999; Jia et al., 2017). Therefore, deciduous trees mainly use water in shallow soil layers, whereas coniferous trees predominantly take up water at deeper soil depth. Also, it was observed that transpiration was greater for coniferous trees (*Pinus tabuliformis* Carrière) than for deciduous trees (*Quercus variabilis* Bl.) (Jia et al., 2017). Hence, one may expect that different tree species may lead to drastically different root channel networks and soil water conditions (e.g., antecedent soil water content) that could substantially influence preferential flow in forest soils (Jarvis, 2007; Merdun et al., 2008; Hardie et al., 2011). The leaching and bioavailability of nutrients, for example, as influenced by soil water flow, could determine soil fertility and forest productivity (Legout et al., 2009). Additionally, preferential flow in soils could affect soil erosion, landslides, and groundwater resources in forest ecosystems (Zehe et al., 2010; Beven and Germann, 2013; Keesstra et al., 2016). Therefore, it is important to characterize the relationships among the tree roots, preferential flow, and solute transport in forest soils.

This study aimed to investigate the features of preferential flow patterns and solute transport in forest soils as well as the relationships among roots, preferential flow, and solute transport in two contrasting forest ecosystems. To do so, we used a rocky mountainous area at the northern China, where soil layer is thin, as our study area. We selected two typical and widely distributed forests ecosystems: a deciduous forest dominated by *Quercus variabilis* and a coniferous forest mainly planted with *Platycladus orientalis* (L.) Franco. Tracer experiments were conducted to investigate the preferential flow pathways and solute transport characteristics in forest soils using dual tracers (Brilliant Blue FCF [BB] and bromide [Br^-]). Using BB allowed us to visualize the preferential flow pathways and identify the stained roots, which we then used to explore the relationships between roots and preferential flow. The measurement of BB and Br^- concentrations in soil profiles was also used to relate the preferential flow to the transport of BB and Br^-. This study highlights the important role of tree roots and tree species in regulating the water and solute transport in forest soils.

Materials and Methods

Experimental Site

Field experiments were performed in the Jiufeng National Forest Park (40°03′54″ N, 116°05′45″ E), located northwest of Beijing, China, and occupying a total area of 811 ha. The park is primarily used for teaching and scientific research. Mount Jiufeng has a maximum elevation of 1153 m and a minimum elevation of 60 m asl. This region is in a typical continental warm temperate zone and has a monsoon climate with a mean annual precipitation of 630 mm and an average annual temperature of 12.5°C, with a record maximum temperature of 41.6°C in July and a record minimum temperature of −19.6°C in January (Jia et al., 2017). Mount Jiufeng has a vegetation cover of approximately 86%, and the majority of its existing forest was planted in the 1950s to the 1960s. The dominant tree species include *Platycladus orientalis*, *Pinus tabuliformis*, *Quercus variabilis*, and *Robinia pseudoacacia* L. (Li et al., 2016; Zhang et al., 2016). In this study, we selected two sites representing two typical forest types, the deciduous forest (DF) site and the coniferous forest (CF) site. At each site, there were two experimental plots. Plot 1 and 2 at the DF site were mainly planted with *Quercus variabilis*, and Plot 3 and 4 at the CF site were dominated by *Platycladus orientalis*. All the plots were less than 300 m asl and were located in flat areas.

To measure soil physicochemical properties, both intact soil cores (100 cm^3) and disturbed soil samples at three depth intervals (0–10 cm, 10–20 cm, and 20–30 cm) were collected at four random spots near the experimental plots at each site. Disturbed soil samples at each depth interval were mixed to obtain a composite sample (approximately 1 kg) for measuring particle size distribution by a laser particle size analyzer (Microtrac S3500) and soil organic content by the dichromate oxidation method (Bai et al., 2011). The intact soil core samples were used to measure initial gravimetric soil water content, bulk density, and total porosity. The selected soil physicochemical properties are shown in Table 1. The soils at the two sites were Luvisols and had mostly a sandy loam texture according to the USDA classification. The bulk density ranged from 1.13 ± 0.11 g cm^{-3} to 1.42 ± 0.16 g cm^{-3} and total porosity was between 46.2 and 57.2%.

Table 1. Physicochemical properties of the soils.

Forest type†	Soil depth	Sand	Silt	Clay	Soil type‡	Initial soil water content	Bulk density	Total porosity	Soil organic content
	cm	%	%	%		%	g cm^{-3}	%	%
DF	0–10	69.6	23.2	7.2	Sandy loam	11.5 ± 0.72	1.18 ± 0.08	55.4 ± 3.12	2.39
	10–20	87.3	8.2	4.5	Sand	9.28 ± 1.02	1.42 ± 0.16	46.2 ± 5.87	1.06
	20–30	71.4	25.9	2.7	Sandy loam	9.00 ± 2.25	1.38 ± 0.12	47.8 ± 4.39	1.16
CF	0–10	61.9	35.0	3.1	Sandy loam	13.6 ± 0.77	1.26 ± 0.05	52.6 ± 2.02	3.37
	10–20	68.4	26.0	5.6	Sandy loam	14.5 ± 1.86	1.13 ± 0.11	57.2 ± 4.30	2.17
	20–30	66.7	26.0	7.3	Sandy loam	14.6 ± 1.89	1.30 ± 0.14	51.0 ± 5.13	1.27

† DF, deciduous forest; CF, coniferous forest.

‡ Soil type was classified using the USDA soil texture classification.

Soil organic content varied from 1.06% at the lower soil depth to 3.37% in the top soil. The initial gravimetric soil water content was 9.00 to 14.6%, indicating the soils were relatively dry (much less than the field capacity) when the tracer experiments were conducted in August and September 2016.

Tracer Experiment

The dual-tracer experiment was performed at each plot to simultaneously characterize the preferential flow patterns and solute transport, similar to earlier studies (Nobles et al., 2010; Schwen et al., 2014; Sheng et al., 2014). Both tracers have advantages and disadvantages. Brilliant Blue is an ionizable organic molecule with charged functional groups and aromatic benzene rings, whereas Br^- is a negative charged inorganic ion (Ketelsen and Meyer-Windel, 1999; Germán-Heins and Flury, 2000). The mobility of BB in soils is rather limited due to its affinity to soil surfaces (Kasteel et al., 2005; Bogner et al., 2008). The sorptive property and vivid color of BB make it an excellent tracer to stain the area of water flow and thus identify preferential flow pathways in soils. It can also approximate the movement of organic molecules as its charge and aromatic characteristics approximately resemble other organic molecules (Nobles et al., 2010; Wang and Zhang, 2011). Conversely, the low background concentration and nonreactive nature of the anion Br^- in soils make it highly suitable for tracing the flow of water and negatively charged nutrient ions in field studies (Flury and Wai, 2003; Sheng et al., 2014). But it often requires extensive soil or water sampling and analyses to identify the preferential flow paths. Due to the contrasting characteristics of BB and Br^-, a study using one tracer will only offer a partial understanding of the water and solute transport in soils. Therefore, the dual tracers (BB and Br^-) were used in the tracer experiments.

Before commencing the tracer experiment, a square steel frame (120 cm by 120 cm) was vertically inserted into the soil to a depth of 15 cm. Fresh leaf litter within the steel frame was then removed without disturbing the underlying humus layer. Afterward, 58 L (equivalent to approximately 40 mm rainfall) of the mixed solution containing BB (5 g L^{-1}) and Br^- (5 g L^{-1}) was uniformly sprayed to the top soil surface within the steel frame at a rate of 50 mm h^{-1} using a rechargeable backpack sprayer, as per the previously established method (Yan and Zhao, 2016; Zhang and Xu, 2016; Zhang et al., 2016). The uniformity coefficient was 0.95, and no visible ponding occurred during the entire tracer application period. Thereafter, the dyed area was covered by a piece of canvas (2 m by 2 m) to prevent evaporation and rainfall infiltration. The maximum daily potential evapotranspiration is about 7 mm at the Mount Jiufeng forest sites (Jia et al., 2017), and the actual transpiration would be less than that as evaporation did not occur in the experimental plots. Thus, infiltration and redistribution (i.e., percolation) were considered to be the primary processes contributing to water flows in our experiments, whereas transpiration played a minor role (i.e., <17.5% of the applied 40-mm water).

After 24 h, the canvas and steel frame were carefully removed. The 24-h period between the tracer application and sampling was selected to allow for adequate percolation of tracer solution for characterizing both infiltration and redistribution of water. Afterward, one-half of the dyed area (120 by 60 cm^2) was used for excavating vertical soil profiles, and the other half for excavating horizontal soil profiles, as shown in Fig. 1. Based on the depth of dyed soil profiles and the location of bedrock, all soil profiles were excavated to a depth of 30 cm (Fig. 1). To avoid any boundary effect, three vertical profiles were collected starting at 20 cm from one edge of the steel frame with a lateral increment of 10 cm at each plot, as shown in Fig. 1. After excavation, each vertical profile was trimmed by a flat-headed shovel. Subsequently, the exposed vertical faces with a size of 100 cm (width) by 30 cm (height) were photographed and corrected for geometric distortion according to the edge points marked by rulers. After the images were taken, soil samples were collected from the vertical

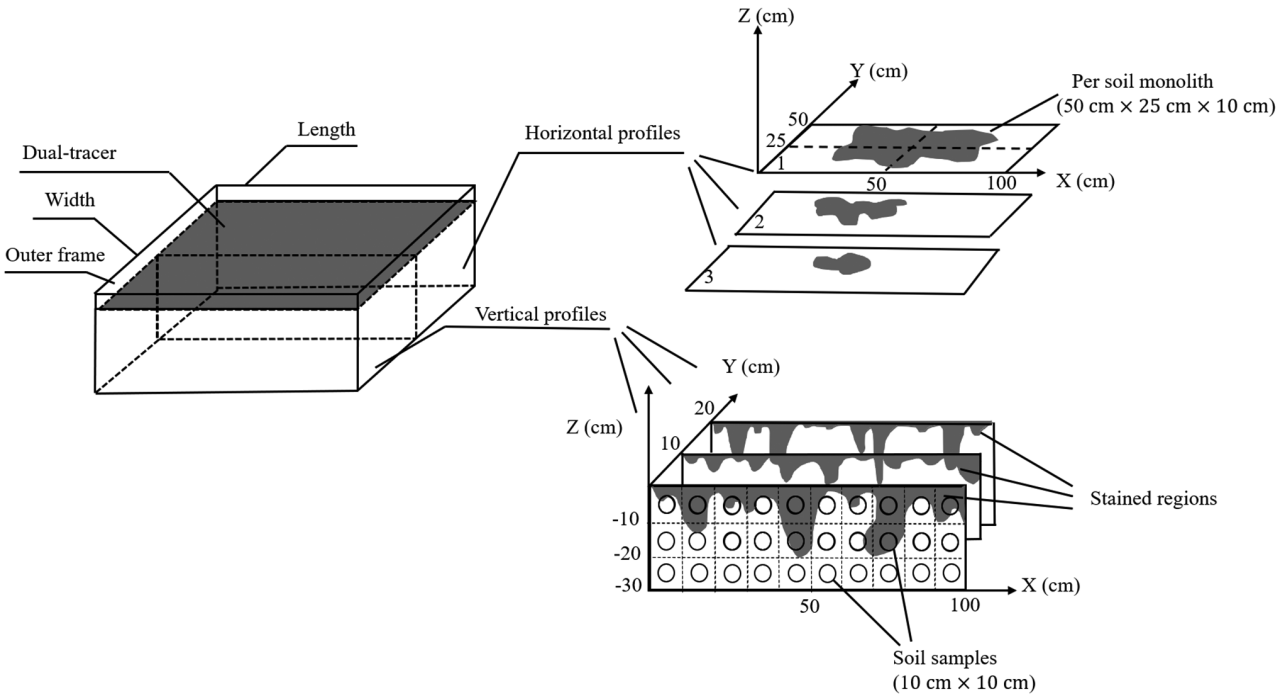

Fig. 1. Tracer experiment setup and sampling scheme.

soil profiles for measuring the concentrations of BB and Br^- using a gridded frame (100 cm by 30 cm) consisting of 30 small grids (10 cm by 10 cm). Approximately 70 g of soil samples was collected from each grid, and 30 soil samples from each vertical soil profile (i.e., 90 soil samples at each plot). Therefore, 360 samples in total were collected from the vertical soil profiles at four plots. The remaining half (120 cm by 60 cm) of the dyed area at each plot was excavated horizontally at a vertical interval of 10 cm (Fig. 1). Three horizontal soil profiles (100 cm by 50 cm) were obtained at each plot, and each horizontal profile was further processed for collecting root samples as described below.

Image Analysis

In the captured images, "stained" and "unstained" areas were distinguished by Photoshop CS6 (Adobe Systems Inc.) according to Nobles et al. (2010) and Koch et al. (2016). Briefly, after geometric correction, the contrast and brightness of each photograph were adjusted. Then, the original photographs were processed on the basis of a threshold brightness value (Williams et al., 2010; Liu and Lennartz, 2015). Finally, the stained pathways were represented in black and isolated from the unstained pathways by visual inspection of the binary images. To characterize the dye pathways in the vertical soil profiles, we used three indices introduced by Flury et al. (1994), van Schaik (2009), and Bargués Tobella et al. (2014).

Dye coverage (DC, %) is the proportion of the dye-stained area to the sum of the stained and unstained areas (Eq. [1]):

$$\mathrm{DC} = 100 \cdot \left(\frac{D}{D + \mathrm{ND}} \right) \quad [1]$$

where D (cm^2) and ND (cm^2) are the dye-stained area and the unstained area, respectively. The dye coverage was calculated according to the percentage of black pixels in each horizontal line in the binary images for each vertical profile.

Preferential flow fraction (PF-fr, %) is the fraction of the total percolation that flows along preferential flow pathways (Eq. [2]):

$$\text{PF-fr} = 100 \cdot \left(1 - \frac{\mathrm{UniFr} \cdot W}{\mathrm{TSA}} \right) \quad [2]$$

where UniFr is the uniform percolation depth (cm) that is defined as the depth at which the dye coverage decreases below 80%, W is the width of the vertical profile (100 cm), and TSA is the total stained area (cm^2).

Length index (LI, %) is the sum of the absolute differences between the dye coverage values of two consecutive depth intervals in a vertical profile. Soils with a high degree of preferential flow will have a higher length index, calculated using Eq. [3]:

$$\mathrm{LI} = \sum_{i=1}^{n} \left| \mathrm{DC}_{i+1} - \mathrm{DC}_i \right| \quad [3]$$

where i represents a given depth interval (or zone) among the n depth intervals for which DC (%) was calculated.

Root Sample Collection and Quantification

Root systems in soils were characterized by a monolith method as described by Perkons et al. (2014) and Wu et al. (2017). Once the dye tracer flowed along the root channels, the surface of roots were stained by the BB dye. Hence, it was assumed that the stained roots contributed to the preferential percolation of water. It was recognized that the staining of roots may also result from the uptake of dyed water due to transpiration. Given that transpiration was minor, as the maximum potential evapotranspiration (~7 mm) (Jia et al., 2017) was <17.5% of the applied water (40 mm), it was reasonable to assume that the staining of roots largely resulted from the water percolation via preferential flow paths. Figure 2 illustrates typical stained soil profiles (Fig. 2a) and fully or partially stained roots (Fig. 2b). To collect the monolith at each plot, each horizontal profile was divided into four equal parts, and each part was excavated as a soil monolith (50 cm by 25 cm by 10 cm) (Fig. 1). Thus, 12 monoliths were collected from each plot, resulting in 48 monoliths in total. Root samples were then collected from the monoliths. As root death is ambiguous and difficult to define in field soils, it was impossible to separate live roots from dead roots (Comas et al., 2000; Sierra et al., 2003). Therefore, the live roots were not distinguished from the dead roots in this study. Once all roots were collected from each monolith, they were sorted by color (i.e., stained and unstained) under natural light. Afterward, the roots with diameter <5 mm were sieved out and then measured with a vernier caliper (Zhang et al., 2016; Wu et al., 2017). Then, the roots were soaked in water to remove the attached soil particles without damaging their structure. Finally,

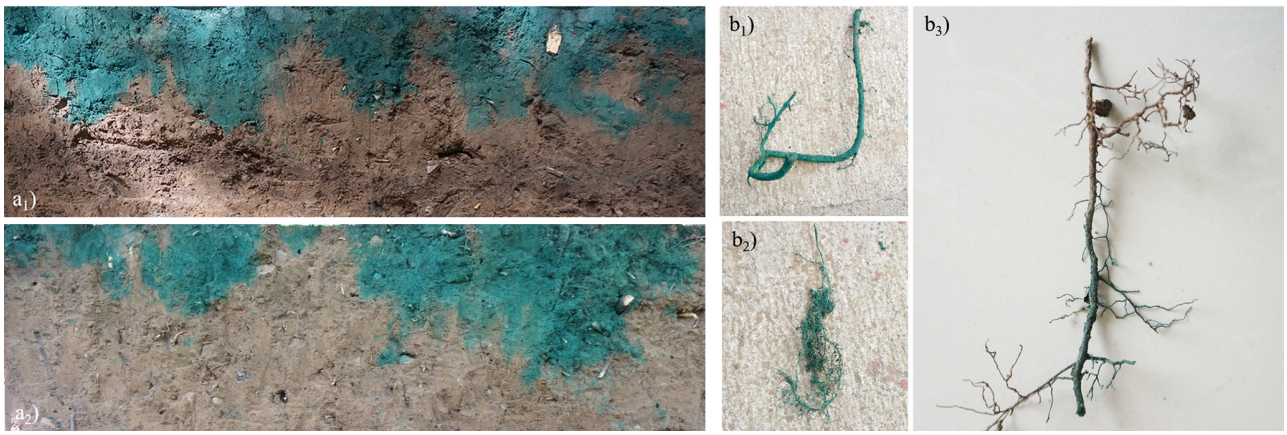

Fig. 2. Example of (a) stained vertical soil profiles and (b) stained roots collected from horizontal soil profiles. Panels a_1 and a_2 show the typical profiles of deciduous forest and coniferous forest, respectively. Panels b_1 and b_2 show the fully stained roots, and Panel b_3 illustrates partially stained roots.

these roots were scanned using an EPSON Expression 1680 1.0. Root length density (RLD)—defined as the total root length (cm) in any sampled soil volume (cm^3)—was measured for each root diameter class in each monolith by WinRHIZO (std 4800) (Yan et al., 2011). The dye was unevenly distributed in each horizontal soil profile. To avoid inaccurate estimation of the stained and unstained RLDs, the total RLD and the RLDs of the stained and unstained roots were estimated in four monoliths at each soil layer and then averaged.

The distribution of stained or unstained RLDs for various root diameter classes was determined using Eq. [4]:

$$\text{Proportion}_{(i)} = \frac{\text{RLD}_{(i)}}{\sum_{i=1}^{5}\text{RLD}_{(i)}} \quad (i = 1,2,3,4,5) \qquad [4]$$

where i is the class of root diameter (d), and $\text{RLD}_{(i)}$ is the stained or unstained RLD for the diameter class i. In this study, the following diameter classes were used: 0 mm < d ≤ 0.50 mm (i = 1), 0.50 mm < d ≤ 1.00 mm (i = 2), 1.00 mm < d ≤ 1.50 mm (i = 3), 1.50 mm < d ≤ 2.00 mm (i = 4), and 2.00 mm < d ≤ 5.00 mm (i = 5).

Laboratory Measurement

The soil samples collected from the vertical soil profiles were dried for 24 h at 105°C, then ground and sieved through a 1-mm mesh for later analyses. For each soil sample, the concentration of BB and Br^- were analyzed as follows. To extract the BB from soil samples, 3 g of each oven-dried soil sample was equilibrated with 30 mL deionized water by shaking for 6 h. The mixture was centrifuged for 1 h at 3000 rpm, and then 10 mL of the supernatant was filtrated through a 0.45-μm filter membrane. The BB concentration in the filtrate was measured by an ultraviolet–visible spectrophotometer at a wavelength of 630 nm (Kasteel et al., 2005). To measure the Br^- concentrations, 10 g of each soil sample was equilibrated with 50 mL deionized water by shaking for 12 h, followed by centrifugation at 3000 rpm for 1 h. The supernatant was then filtrated using a qualitative filter paper. The Br^- concentration in the filtrate was measured by an ion meter (PXSJ-216F, Shanghai INESA & Scientific Instrument Co., Ltd.) (Sheng et al., 2014; Zhang et al., 2015). Then the concentrations of BB and Br^- in soil samples were calculated as the tracer mass per unit mass of soil (mg kg^{-1} soil).

As the measured BB and Br^- concentrations varied substantially from each other, to better understand their interrelationship, their concentrations were transformed into the relative concentration (C', %) using Eq. [5] (Schwen et al., 2014; Liu and Lennartz, 2015):

$$C' = \frac{C - C_{\min}}{C_{\max} - C_{\min}} \qquad [5]$$

where C is the tracer concentration (mg kg^{-1} soil) in soil samples collected in each 10-cm by 10-cm grid, and $C_{\max}$ and $C_{\min}$ are the maximum and minimum tracer concentrations (mg kg^{-1} soil) in each soil profile, respectively.

Data Analysis

Spearman's correlation coefficients were used to quantify the correlation among the BB concentration, the Br^- concentration, and the amount of roots in soils. Normal distribution of the experimental datasets was assessed with the Kolmogorov–Smirnov test. The difference between the RLD values of stained roots and unstained roots, between the total RLD values at the DF and CF sites, and between the tracer (BB and Br^-) concentrations at the DF and CF sites was tested by a nonparametric Mann–Whitney U test using the least significant difference (P < 0.05). The difference between the preferential path indices at the DF and CF sites was analyzed by the independent-sample t test (P < 0.05). All statistical analyses were performed using the IBM SPSS Statistics software (version 22.0; IBM Corporation). Additionally, the figures were plotted by the Origin Pro 8.0 software (OriginLab).

Results

Patterns of Flow Paths and Solute Transport

Mean RLD in all plots decreased with soil depth and was close to zero at the depth of 30 cm (Table 2). The mean total stained area of the CF plots (1241 cm^2) was significantly greater than that of the DF plots (991 cm^2) (P < 0.05). Additionally, the PF-fr values reflected the fraction of the preferential pathways in the overall soil profiles and were higher at the CF site than at the DF site (P < 0.05). Moreover, the mean length index at the CF site (184) was significantly greater than that at the DF site (150) (P < 0.05).

In all plots, the maximum, minimum, and mean value of BB and Br^- concentrations generally decreased with soil depth (Table 3). The BB and Br^- concentrations ranged from 0 to 557 mg kg^{-1} soil and from 3.39 to 1322 mg kg^{-1} soil, respectively. In addition, the arithmetic means of BB and Br^- concentrations in the 0- to 30-cm soil profiles were 55.5 and 374 mg kg^{-1} soil, respectively. The minimum BB concentrations were always lower than the minimum Br^- concentrations in the 20- to 30-cm soil layer, indicating that Br^- was transported deeper into the soil profiles than BB in all plots (Table 3). Additionally, the mean concentrations of Br^- and BB in the 20- to 30-cm soil layer at the CF site were significant greater than those at the DF site (P < 0.05).

The distributions of BB and Br^- in the soil profiles are presented in Fig. 3. Notably, Br^- was transported more extensively than BB in all the plots. Preferential pathways existed and facilitated the transport of both two tracers to the deeper soil layers by bypassing certain parts of the soil matrix. The concentrations of BB and Br^- in preferential flow pathways were significantly higher than those in the surrounding soil matrix. The correlations between the relative concentration of BB and Br^- were significant (P < 0.01), and the Spearman's coefficient was 0.846 in the soil layer 0 to 30 cm.

Features of Roots in Various Soil Layers and Root Diameters

The total RLD decreased with soil depth in all plots (Fig. 4). The mean RLD in the 0- to 30-cm soil layer at the DF site was 3.50 ± 1.58 mm cm^{-3}, which was significantly greater than that at the CF site (P < 0.05). The unstained roots in every root diameter class were observable in the entire soil profiles (Fig. 4 and 5). The maximum proportion of the stained roots appeared in the 0- to 10-cm layer, ranging from 86.0 to 99.2%. Additionally, in

the 0- to 20-cm soil layer, the mean RLD of the unstained roots was 1.03 mm cm^{-3}, which was significantly smaller than that of the stained roots ($P < 0.05$). The proportion of the stained roots to total roots ranged from 51.1 to 68.9% in all plots in 0- to 30-cm soil layer. Generally, the percentages of the stained finer roots (<1 mm) accounted for a majority of the total stained roots in each soil layer. The distributions of RLD among various root diameter classes were similar for the stained and unstained roots. Additionally, the proportion of fine roots (<1 mm diam.) to total roots at the DF site was significantly higher than that at the CF site ($P < 0.05$).

Relationships among Preferential Paths, Solute Transport, and Roots

The length index values characterizing the degree of preferential flows were positively related to the concentrations of the two tracers in the 20- to 30-cm soil layer ($P = 0.033$ and $R^2 = 0.623$ for BB; and $P = 0.013$ and $R^2 = 0.555$ for Br^-) (Fig. 6). The correlation coefficient between the total RLD values and dye coverage values was 0.664 ($P < 0.05$), while the correlations between the total RLD values and the BB or Br^- concentrations were significant, with a Spearman's coefficient of 0.720 ($P < 0.01$) and 0.783 ($P < 0.01$), respectively. The dye coverage values and both tracer concentrations increased with increasing total RLD values at both sites (Fig. 7). Based on the value of R^2, the total RLD values and the tracer concentrations were better linearly correlated at the CF site than at the DF site. Generally, at the CF site, a soil layer with a root amount similar to that at the DF site had greater tracer concentrations.

Discussion

The decreasing trend of the dye coverages and tracer concentrations with increasing soil depth (Tables 2 and 3) agrees with the studies of Nobles et al. (2010) and Schwen et al. (2014).

Table 2. Characteristics of dye pathways in all plots.

Plot†	Profile	TSA‡	PF-fr‡	LI‡	Soil layer	DC‡		
						Mean	SD	CV
		cm^2	%		cm	%		
DF Plot 1	Profile 1	1360	26.1	159	0–10	82.5	9.24	11.2
	Profile 2	1069	54.7	170	10–20	34.2	18.6	54.3
	Profile 3	1106	38.4	139	20–30	1.13	1.27	112.6
	Mean	1178	39.7	156				
DF Plot 2	Profile 1	654	27.9	147	0–10	72.7	23.3	32.1
	Profile 2	957	33.3	129	10–20	7.53	8.20	109
	Profile 3	799	40.1	153	20–30	0.14	0.12	83.3
	Mean	803	33.8	143				
CF Plot 3	Profile 1	1263	52.5	175	0–10	79.0	6.79	8.60
	Profile 2	1281	68.6	181	10–20	44.6	13.9	31.1
	Profile 3	1391	68.8	208	20–30	7.62	6.58	86.4
	Mean	1312	63.3	188				
CF Plot 4	Profile 1	1176	37.1	162	0–10	78.0	15.7	20.2
	Profile 2	1174	60.4	178	10–20	29.3	7.32	25.0
	Profile 3	1161	60.3	200	20–30	9.74	5.53	56.8
	Mean	1170	52.6	180				

† DF, deciduous forest; CF, coniferous forest.

‡ TSA, total stained area; PF-fr, preferential flow fraction; LI, length index; DC, dye coverage.

Table 3. Statistical characteristics of Brilliant Blue (BB) and Br^- concentrations in four plots.

Plot†	Soil depth	BB‡				Br^-‡			
		Max.	Min.	Mean	SD	Max.	Min.	Mean	SD
	cm	mg kg^{-1} soil							
DF Plot 1	0–10	557	11.6	240	157	1092	391	710	162
	10–20	206	0.71	44.9	53.4	688	46.2	399	189
	20–30	5.05	0.04	1.09	1.23	301	9.43	127	86.1
DF Plot 2	0–10	406	0.00	118	86.2	956	62.3	654	251
	10–20	15.4	0.00	1.72	3.65	401	7.83	95.8	110
	20–30	6.48	0.00	0.78	1.53	220	3.39	25.6	48.9
CF Plot 3	0–10	321	1.10	110	93.3	961	183	613	221
	10–20	209	0.43	41.9	54.3	738	11.4	393	231
	20–30	116	0.06	13.9	30.0	781	7.03	265	233
CF Plot 4	0–10	278	4.51	80.3	70.4	1322	305	803	258
	10–20	59.8	0.04	6.78	16.3	1045	13.6	293	237
	20–30	103	0.00	6.69	20.2	601	7.93	107	149

† DF, deciduous forest; CF, coniferous forest.

‡ Max., Min., and SD are the maximum, minimum, and standard deviation of data series.

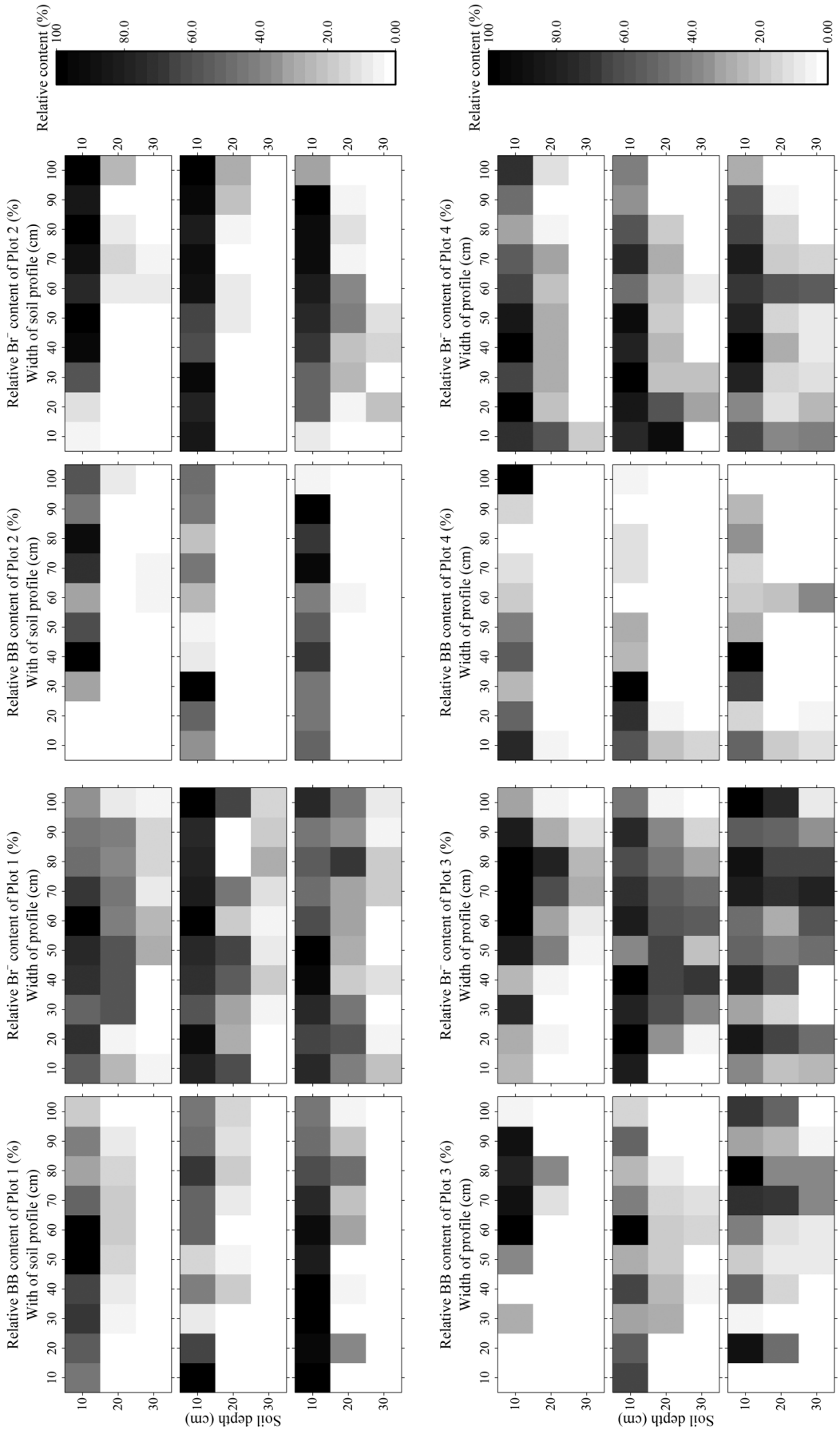

Fig. 3. Leaching characteristics of Brilliant Blue FCF (BB) and Br^- in the soil profiles of Plots 1 and 2 at the deciduous forest site and Plots 3 and 4 at the coniferous forest site.

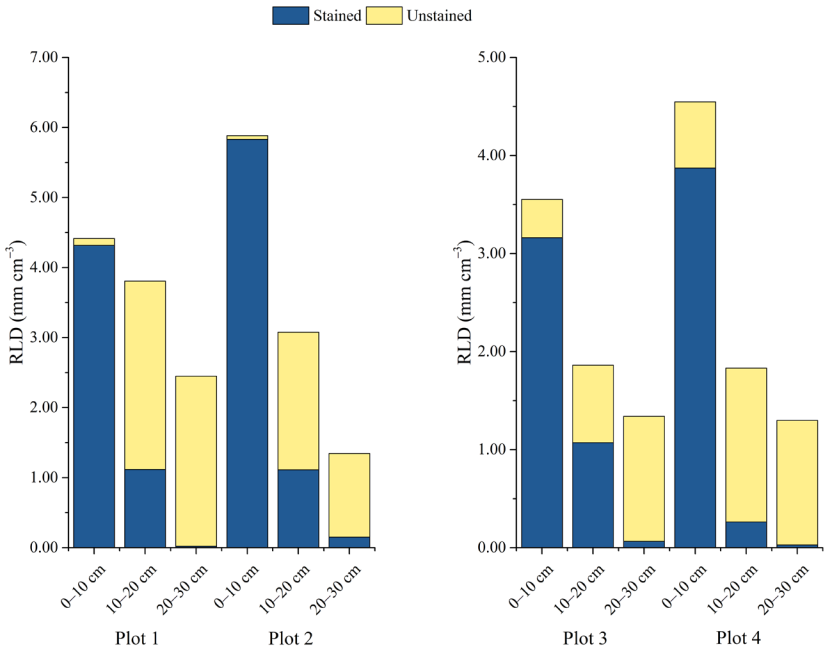

Fig. 4. Changes in the root length density (RLD) of the stained or unstained roots with soil depth for Plots 1 and 2 at the deciduous forest site and Plots 3 and 4 at the coniferous forest site.

This observation was primarily due to a greater amount of water absorption in the shallower soil depth during percolation, as supported by the fact that the tracers (BB and Br^-) were concentrated in the 0- to 20-cm soil layers and the stained RLD was significantly greater than the unstained RLD ($P < 0.05$) (Fig. 3 and 4). Another reason could be due to the decreasing biological activity with increasing soil depth, as the soil rhizosphere exudates from microorganisms and plant roots could enhance soil aggregation, thus forming inter-aggregate macropores, serving as preferential flow paths (Fageria and Stone, 2006; Ghestem et al., 2011). Additionally, root channels could create well-connected networks that contribute to water percolation (Noguchi et al., 1997; Sidle et al., 2001; Newman et al., 2004).

Compared with BB, a broader and deeper transport of Br^- through soil profiles was observed in this study (Table 3 and Fig. 3). During water percolation, Br^- and BB tracers would interact with soil surfaces. Because BB is an ionic organic molecule containing three negatively charged sulfonate groups, one positively charged amine group, and five aromatic benzene rings, BB would sorb to the charged soil surfaces (e.g., clay and metal oxides) and organic matters rich in aromatic structures (e.g., humic substances) via electrostatic interaction and π–π or cation–π electron donor–acceptor interactions (Ketelsen and Meyer-Windel, 1999; Germán-Heins and Flury, 2000; Zhu et al., 2004). Thus, one would expect a much greater affinity of BB to soils and consequently a lower mobility of BB in soils than that of Br^- (Flury and Flühler, 1995), which is corroborated by this and other studies (Öhrström et al., 2004; Bogner et al., 2008; Nobles et al., 2010). Schwen et al. (2014) performed tracer experiments in grassland and cropland soils by applying 70-mm depth of water, observing much more divergent transport behaviors of BB and Br^- in the 0- to 30-cm soil layer than we saw in our study (Fig. 3). One of the underlying reasons for this difference could be a greater extent of macropore flows in forest soils than in grassland and cropland soils (Bachmair et al., 2009; Alaoui et al., 2011). As water tends to move along pathways of least resistance (Wang and Zhang, 2011), it was expected that the tracer solutions in our study would flow through the macropores, thus bypassing large parts of soil matrix. As a result, there was less contact time and interaction of the tracers with soil matrix and subsequently less difference in the transport of BB and Br^- compared with that of Schwen et al. (2014).

The unstained roots were found throughout the soil profiles, even in the 0- to 10-cm soil layers (Fig. 4), indicating that not all of the roots acted as preferential channels for water percolation. This result supports Bachmair et al. (2009), who found that not all of the existing roots facilitated the water transport in forest soils. Also, large amounts of finer roots could contribute more to the preferential transport of solutes, as indicated by a greater proportion of dye-stained fine roots (<1 mm) (Fig. 5), which likely resulted from the greater root and soil contact area for fine roots as well as the abundance and connectivity of these finer roots.

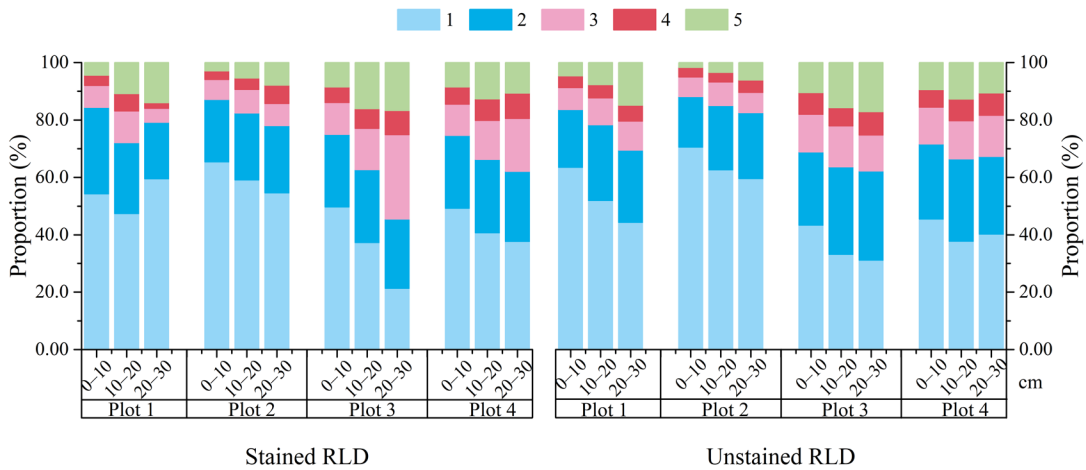

Fig. 5. Proportions of root length density (RLD) for the stained and unstained roots in various diameter (*d*) classes (1: 0 mm < *d* ≤ 0.50 mm; 2: 0.50 mm < *d* ≤ 1.00 mm; 3: 1.00 mm < *d* ≤ 1.50 mm; 4: 1.50 mm < *d* ≤ 2.00 mm; 5: 2.00 mm < *d* ≤ 5.00 mm).

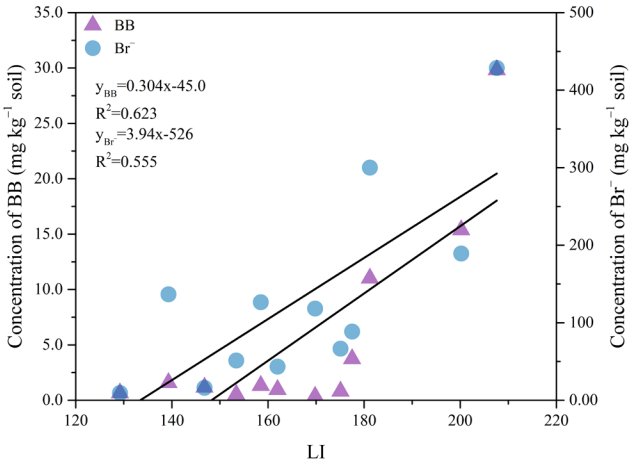

Fig. 6. Correlations between the features of preferential paths and solutes concentrations in the 20- to 30-cm soil layer. BB, Brilliant Blue; LI, length index.

The mean concentrations of BB and Br^- were significantly higher at the CF site, where the soils had a higher degree of preferential flow, than at the DF site in the 20- to 30-cm soil layers ($P < 0.05$) (Table 2 and 3, Fig. 6). Thus, the tracers were more concentrated to the preferential flow paths at the CF site than at the DF site. Conversely, the tracers were mainly distributed in the upper soil lays, lowering the mean tracer concentrations at the DF site. Additionally, there was a close relationship between the tracer concentrations and the total RLD, demonstrating the important role of root channels in transporting the solutes (Fig. 7). It is also possible that greater activity of soil organisms in the rhizosphere contributes to greater degree of preferential flow along roots. Our results indicated that compared with the DF site, the preferential paths could result in greater leaching of the solutes at the CF site with surprisingly lower amounts of total RLD, a lower proportion of fine roots (<1 mm), and a greater proportion of roots with a diameter between 1 and 5 mm ($P < 0.05$) in the 0- to 30-cm soil layers (Fig. 4 and 5). The discrepancy in the greater tracer concentrations with lower RLD at the CF site than at the DF site points to the possibility of the important role played by the root systems of various tree species. It was reported that the various morphometric features of roots could profoundly affect the water infiltration and distribution in soils (Jiang et al., 2018). Ghestem et al. (2011) also pointed out that root systems with relative large and shallow roots well connected with plant stems could facilitate lateral subsurface flows, but root systems with larger vertical taproots and thinner lateral roots would enhance vertical water flow along the thick taproots. As coniferous trees have well-developed deeper roots at the 40- to 60-cm soil depth and deciduous trees have well-developed roots in shallow soils (0–25 cm) (Bauhus and Messier, 1999; Jia et al., 2017), the fine roots (<1 mm) in the shallow soil (0–30 cm) may enhance the lateral surface flow at the DF site, thus reducing the vertical preferential flows. However, at the CF site, the larger roots (1–5 mm) could effectively allow water to percolate downward, thus enhancing the preferential flows. This study was limited in the sense that the intact root systems were not characterized in situ and thus precluded the possibility of corroborating the preferential flow patterns with in situ root system characteristics. Thus, future experiments should be directed to examine the root systems and their interrelationship with water flow in the subsurface using nondestructive in situ characterization tools such as ultra-fast neutron tomography (Tötzke et al., 2017), ground penetrating radar (Guo et al., 2013), and noninvasive magnetic resonance (Pflugfelder et al., 2017).

Several other compounding factors may also need to be considered in future tracer experiments. As active and dynamic interactions exist between roots and soil water (Legates et al., 2011; Yang et al., 2014; Zhao et al., 2014; Wang et al., 2015), the active root uptake of water could substantially influence water redistribution within the soil profiles after infiltration. Nonetheless, this factor could be minor in the short 24-h period as the transpiration was less than 17.5% of the percolated water amount (i.e., 40 mm). Meanwhile, the channels formed by dead and decayed roots could affect the movement of water in soils, and thus it would be ideal that the live and dead roots be distinguished and separately measured. Furthermore, the root systems could influence the antecedent soil moisture that is closely related to preferential flows (Jarvis, 2007; Merdun et al., 2008; Hardie et al., 2011). It was reported that the water and solute transport in dry soils is more pronounced than in wetter soils (Shipitalo and Edwards, 1996; Merdun et al., 2008; Tang et al.,

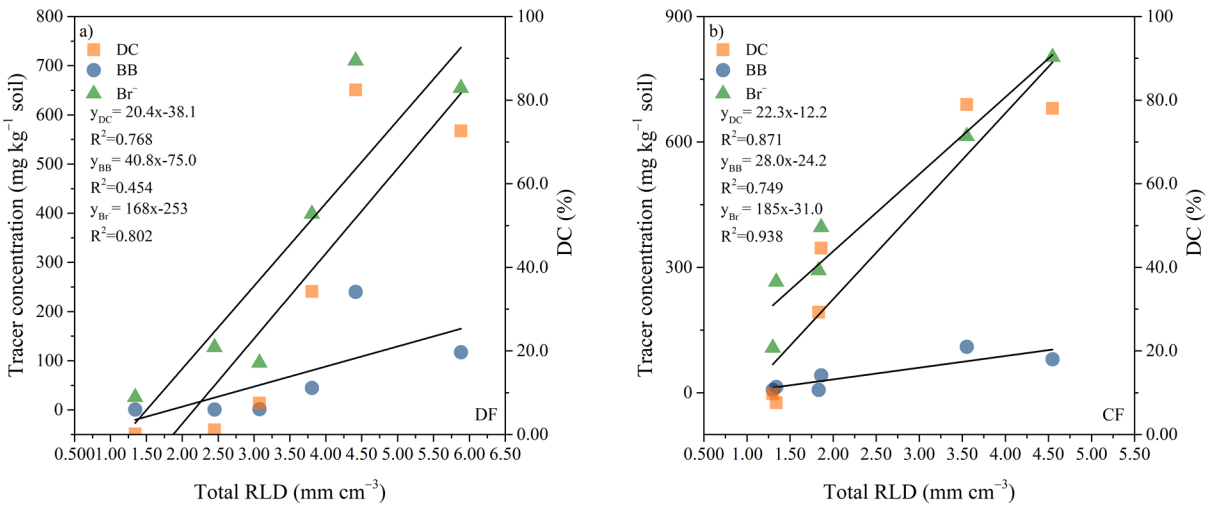

Fig. 7. Correlations between the total root length density (RLD) and the tracer concentrations or the dye coverage (DC) in the 0- to 30-cm soil layers at the (a) deciduous forest (DF) and (b) coniferous forest (CF) sites. BB, Brilliant Blue.

2012). However, others found that the wetter soils could reduce lateral flow into the soil matrix and increase the deeper percolation of water and solute via vertical preferential flows (Beven and Germann, 1982; Jarvis, 2007; Greve et al., 2010). As the CF site had a greater initial soil water content than the DF site (Table 1), our results appear to support the latter finding. It is interesting to note that the greater transpiration of coniferous trees (e.g., *Pinus tabuliformis*) compared with deciduous trees (e.g., *Quercus variabilis*) (Jia et al., 2017) did not result in drier soil conditions in the shallow soil at the CF site, likely because coniferous trees mainly use soil water at the deeper soil depth, but deciduous trees predominantly absorb water at the shallow soil depth. This observation was also corroborated by the RLD measurements (Fig. 4 and 5), as previously discussed. Hence, the influences of antecedent soil water content, as modulated by plant root systems and transpiration, should be further studied in future tracer experiments.

Finally, soil structure may play an important role in controlling the water and solute transport. The greater preferential flow and tracer transport at the CF sites may be partly explained by the stratification of soil porosity in addition to the difference in root systems. The 0- to 10-cm soil layer at the CF site had greater bulk density and lower porosity than the 10- to 20-cm soil layer, but the opposite was found at the DF site (Table 1). Thus, the hydraulic conductivity would be lower in the 0- to 10-cm soil layer than in the 10- to 20-cm soil layer at the CF site, and vice versa at the DF site. As wetting front instability and preferential flow formation are enhanced when a less permeable layer is overlying a coarser layer (Morales et al., 2010), the preferential flow would be more pronounced at the CF site. This alternative explanation points to the important role of soil structural heterogeneity in governing the water and solute transport. Future studies should integrate physical, chemical, and biological factors such as soil texture and structure, initial soil water content, tracer sorption to soils, and intact root systems of varying tree species.

Conclusion

Our dual-tracer (BB and Br^-) experiments demonstrated that both BB and Br^- were mainly accumulated in the soil layers that contained large amounts of roots in forest soils. Thus, the roots played an important role in solute leaching in soils, probably through preferential flows. Only part of the roots facilitated the preferential flows, however. The finer roots accounted for the major portion of the RLD and also contributed more to preferential pathways. Intriguingly, the preferential flows were greater in the coniferous forest soil than in the deciduous forest soil, indicating the important role of tree species and forest composition on the preferential flows in forest ecosystems. These findings improve our understanding of the effects of tree roots on the water percolation and solute leaching in forest ecosystems. Future studies should consider the effects of antecedent soil water content and variable root system structures on preferential flows of water and solutes using advanced in situ characterization tools such as ultra-fast neutron tomography, ground penetrating radar, and noninvasive magnetic resonance. More tracer experiments could also be conducted in various forest communities by considering tree species composition or using tracers, such as nano- or micrometer-sized TiO_2 (Liu and Lennartz, 2015; Koch et al., 2016), that have transport characteristics in soil pores distinct from those of dye tracers and conservative inorganic tracers.

Acknowledgments

This study was supported by the National Natural Science Foundation of China (41741024), Graduate Training and Development Program of Beijing Municipal Commission of Education (BLCXY201623), the National Natural Science Foundation of China (41271044), and grants from the Beijing Municipal Education Commission (CEFF-PXM2018_014207_000024).

References

Alaoui, A., U. Caduff, H.H. Gerke, and R. Weingartner. 2011. Preferential flow effects on infiltration and runoff in grassland and forest soils. Vadose Zone J. 10:367–377. doi:10.2136/vzj2010.0076

Archer, N.A.L., J.N. Quinton, and T.M. Hess. 2002. Below-ground relationships of soil texture, roots and hydraulic conductivity in two-phase mosaic vegetation in south-east Spain. J. Arid Environ. 52:535–553. doi:10.1006/jare.2002.1011

Bachmair, S., M. Weiler, and G. Nützmann. 2009. Controls of land use and soil structure on water movement: Lessons for pollutant transfer through the unsaturated zone. J. Hydrol. 369:241–252. doi:10.1016/j.jhydrol.2009.02.031

Bai, J., R. Xiao, B. Cui, K. Zhang, Q. Wang, X. Liu, et al. 2011. Assessment of heavy metal pollution in wetland soils from the young and old reclaimed regions in the Pearl River estuary, South China. Environ. Pollut. 159:817–824. doi:10.1016/j.envpol.2010.11.004

Bargués Tobella, A., H. Reese, A. Almaw, J. Bayala, A. Malmer, H. Laudon, and U. Ilstedt. 2014. The effect of trees on preferential flow and soil infiltrability in an agroforestry parkland in semiarid Burkina Faso. Water Resour. Res. 50:3342–3354. doi:10.1002/2013WR015197

Bauhus, J., and C. Messier. 1999. Soil exploitation strategies of fine roots in different tree species of the southern boreal forest of eastern Canada. Can. J. For. Res. 29:260–273. doi:10.1139/cjfr-29-2-260

Beven, K., and P.F. Germann. 1982. Macropores and water flow in soils. Water Resour. Res. 18:1311–1325. doi:10.1029/WR018i005p01311

Beven, K., and P.F. Germann. 2013. Macropores and water flow in soils revisited. Water Resour. Res. 49:3071–3092. doi:10.1002/wrcr.20156

Bogner, C., B. Wolf, M. Schlather, and B. Huwe. 2008. Analysing flow patterns from dye tracer experiments in a forest soil using extreme value statistics. Eur. J. Soil Sci. 59:103–113. doi:10.1111/j.1365-2389.2007.00974.x

Comas, L.H., D.M. Eissenstat, and A.N. Lakso. 2000. Assessing root death and root system dynamics in a study of grape canopy pruning. New Phytol. 147:171–178. doi:10.1046/j.1469-8137.2000.00679.x

Devitt, D.A., and S.D. Smith. 2002. Root channel macropores enhance downward movement of water in a Mojave Desert ecosystem. J. Arid Environ. 50:99–108. doi:10.1006/jare.2001.0853

Elçi, A., and F.J. Molz. 2009. Identification of lateral macropore flow in a forested riparian wetland through numerical simulation of a subsurface tracer experiment. Water Air Soil Pollut. 197:149–164. doi:10.1007/s11270-008-9798-5

Fageria, N.K., and L.F. Stone. 2006. Physical, chemical, and biological changes in the rhizosphere and nutrient availability. J. Plant Nutr. 29:1327–1356. doi:10.1080/01904160600767682

Flury, M., and H. Flühler. 1995. Tracer characteristics of Brilliant Blue FCF. Soil Sci. Soc. Am. J. 59:22–27. doi:10.2136/sssaj1995.03615995005900010003x

Flury, M., H. Flühler, W.A. Jury, and J.J. Leuenberger. 1994. Susceptibility of soils to preferential flow of water: A field study. Water Resour. Res. 30:1945–1954. doi:10.1029/94WR00871

Flury, M., and N.N. Wai. 2003. Dyes as tracers for vadose zone hydrology. Rev. Geophys. 41:1002. doi:10.1029/2001RG000109

Germán-Heins, J., and M. Flury. 2000. Sorption of Brilliant Blue FCF in soils affected by pH and ionic strength. Geoderma 97:87–101. doi:10.1016/S0016-7061(00)00027-6

Ghestem, M., R.C. Sidle, and A. Stokes. 2011. The influence of plant root systems on subsurface flow: Implications for slope stability. Bioscience 61:869–879. doi:10.1525/bio.2011.61.11.6

Greve, A., M.S. Andersen, and R.I. Acworth. 2010. Investigations of soil cracking and preferential flow in a weighing lysimeter filled with cracking clay soil. J. Hydrol. 393:105–113. doi:10.1016/j.jhydrol.2010.03.007

Guo, L., H. Lin, B. Fan, X. Cui, and J. Chen. 2013. Impact of root water content on root biomass estimation using ground penetrating radar: Evidence from forward simulations and field controlled experiments. Plant Soil 371:503–520. doi:10.1007/s11104-013-1710-4

Hardie, M.A., W.E. Cotching, R.B. Doyle, G. Holz, S. Lisson, and K. Mattern. 2011. Effect of antecedent soil moisture on preferential flow in a texture-contrast soil. J. Hydrol. 398:191–201. doi:10.1016/j.jhydrol.2010.12.008

Jarvis, N.J. 2007. A review of non-equilibrium water flow and solute transport in soil macropores: Principles, controlling factors, and consequences for water quality. Eur. J. Soil Sci. 58:523–546. doi:10.1111/j.1365-2389.2007.00915.x

Jia, G., Z. Liu, L. Chen, and X. Yu. 2017. Distinguish water utilization strategies of trees growing on earth-rocky mountainous area with transpiration and water isotopes. Ecol. Evol. 7:10640–10651. doi:10.1002/ece3.3584

Jiang, X., W. Liu, C. Chen, J. Liu, Z. Yuan, B. Jin, and X. Yu. 2018. Effects of three morphometric features of roots on soil water flow behavior in three sites in china. Geoderma 320:161–171. doi:10.1016/j.geoderma.2018.01.035

Kasteel, R., M. Burkhardt, S. Giesa, and H. Vereecken. 2005. Characterization of field tracer transport using high-resolution images. Vadose Zone J. 4:101–111. doi:10.2136/vzj2005.0101dup

Keesstra, S., P. Pereira, A. Novara, E.C. Brevik, C. Azorin-Molina, L. Parras-Alcántara, et al. 2016. Effects of soil management techniques on soil water erosion in apricot orchards. Sci. Total Environ. 551-552:357–366. doi:10.1016/j.scitotenv.2016.01.182

Ketelsen, H., and S. Meyer-Windel. 1999. Adsorption of Brilliant Blue FCF by soils. Geoderma 90:131–145. doi:10.1016/S0016-7061(98)00119-0

Koch, S., P. Kahle, and B. Lennartz. 2016. Visualization of colloid transport pathways in mineral soils using titanium (IV) oxide as a tracer. J. Environ. Qual. 45:2053–2059. doi:10.2134/jeq2016.04.0131

Laine-Kaulio, H., S. Backnäs, T. Karvonen, H. Koivusalo, and J.J. Mcdonnell. 2014. Lateral subsurface stormflow and solute transport in a forested hillslope: A combined measurement and modeling approach. Water Resour. Res. 50:8159–8178. doi:10.1002/2014WR015381

Laine-Kaulio, H., S. Backnäs, H. Koivusalo, and A. Laurén. 2015. Dye tracer visualization of flow patterns and pathways in glacial sandy till at a boreal forest hillslope. Geoderma 259–260:23–34. doi:10.1016/j.geoderma.2015.05.004

Legates, D.R., R. Mahmood, D.F. Levia, T.L. Deliberty, S.M. Quiring, C. Houser, and F.E. Nelson. 2011. Soil moisture: A central and unifying theme in physical geography. Prog. Phys. Geogr. 35:65–86. doi:10.1177/0309133310386514

Legout, A., C. Legout, C. Nys, and E. Dambrine. 2009. Preferential flow and slow convective chloride transport through the soil of a forested landscape (Fougères, France). Geoderma 151:179–190. doi:10.1016/j.geoderma.2009.04.002

Leung, A.K., A. Garg, J.L. Coo, C.W.W. Ng, and B.C.H. Hau. 2015. Effects of the roots of *Cynodon dactylon* and *Schefflera heptaphylla* on water infiltration rate and soil hydraulic conductivity. Hydrol. Processes 29:3342–3354. doi:10.1002/hyp.10452

Li, X., J. Niu, L. Zhang, Q. Xiao, G.E. Mcpherson, N. van Doorn, and C. Meng. 2016. A study on crown interception with four dominant tree species: A direct measurement. Hydrol. Res. 47:857–868. doi:10.2166/nh.2015.066

Liu, H., and B. Lennartz. 2015. Visualization of flow pathways in degraded peat soils using titanium dioxide. Soil Sci. Soc. Am. J. 79:757–765. doi:10.2136/sssaj2014.04.0153

Merdun, H., R. Meral, and A. Riza Demirkiran. 2008. Effect of the initial soil moisture content on the spatial distribution of the water retention. Eurasian Soil Sci. 41:1098–1106. doi:10.1134/S1064229308100128

Morales, V.L., J.Y. Parlange, and T.S. Steenhuis. 2010. Are preferential flow paths perpetuated by microbial activity in the soil matrix? a review. J. Hydrol. 393:29–36. doi:10.1016/j.jhydrol.2009.12.048

Moret, D., and J.L. Arrúe. 2007. Dynamics of soil hydraulic properties during fallow as affected by tillage. Soil Tillage Res. 96:103–113. doi:10.1016/j.still.2007.04.003

Newman, B.D., B.P. Wilcox, and R.C. Graham. 2004. Snowmelt-driven macropore flow and soil saturation in a semiarid forest. Hydrol. Processes 18:1035–1042. doi:10.1002/hyp.5521

Nimmo, J.R. 2012. Preferential flow occurs in unsaturated conditions. Hydrol. Processes 26:786–789. doi:10.1002/hyp.8380

Nobles, M.M., L.P. Wilding, and H.S. Lin. 2010. Flow pathways of bromide and Brilliant Blue FCF tracers in caliche soils. J. Hydrol. 393:114–122. doi:10.1016/j.jhydrol.2010.03.014

Noguchi, S., A.R. Nik, B. Kasran, M. Tani, T. Sammori, and K. Morisada. 1997. Soil physical properties and preferential flow pathways in tropical rain forest, Bukit Tarek, peninsular Malaysia. J. For. Res. 2:115–120. doi:10.1007/BF02348479

Öhrström, P., Y. Hamed, M. Persson, and R. Berndtsson. 2004. Characterizing unsaturated solute transport by simultaneous use of dye and bromide. J. Hydrol. 289:23–35. doi:10.1016/j.jhydrol.2003.10.014

Perkons, U., T. Kautz, D. Uteau, S. Peth, V. Geier, K. Thomas, et al. 2014. Root-length densities of various annual crops following crops with contrasting root systems. Soil Tillage Res. 137:50–57. doi:10.1016/j.still.2013.11.005

Pflugfelder, D., R. Metzner, D.V. Dusschoten, R. Reichel, S. Jahnke, and R. Koller. 2017. Non-invasive imaging of plant roots in different soils using magnetic resonance imaging (MRI). Plant Methods 13:102. doi:10.1186/s13007-017-0252-9

Schwen, A., J. Backus, Y. Yang, and O. Wendroth. 2014. Characterizing land use impact on multi-tracer displacement and soil structure. J. Hydrol. 519:1752–1768. doi:10.1016/j.jhydrol.2014.09.028

Sheng, F., H. Liu, K. Wang, R. Zhang, and Z. Tang. 2014. Investigation into preferential flow in natural unsaturated soils with field multiple-tracer infiltration experiments and the active region model. J. Hydrol. 508:137–146. doi:10.1016/j.jhydrol.2013.10.048

Shipitalo, M.J., and W.M. Edwards. 1996. Effects of initial water content on macropore/matrix flow and transport of surface-applied chemicals. J. Environ. Qual. 25:662–670. doi:10.2134/jeq1996.00472425002500040005x

Sidle, R.C., S. Noguchi, Y. Tsuboyama, and K. Laursen. 2001. A conceptual model of preferential flow systems in forested hillslopes: Evidence of self-organization. Hydrol. Processes 15:1675–1692. doi:10.1002/hyp.233

Sierra, C.A., J.I. Del Valle, and S.A. Orrego. 2003. Accounting for fine root mass sample losses in the washing process: A case study from a tropical montane forest of Colombia. J. Trop. Ecol. 19:599–601. doi:10.1017/S0266467403003663

Stone, W.W., and J.T. Wilson. 2006. Preferential flow estimates to an agricultural tile drain with implications for glyphosate transport. J. Environ. Qual. 35:1825–1835. doi:10.2134/jeq2006.0068

Tang, J., B. Zhu, T. Wang, X. Cheng, M. Gao, and H. Lin. 2012. Subsurface flow processes in sloping cropland of purple soil. J. Mt Sci. 9:1–9. doi:10.1007/s11629-012-2199-7

Tötzke, C., N. Kardjilov, I. Manke, and S.E. Oswald. 2017. Capturing 3D water flow in rooted soil by ultra-fast neutron tomography. Sci. Rep. 7:6192. doi:10.1038/s41598-017-06046-w

van der Heijden, G., A. Legout, B. Pollier, C. Bréchet, J. Ranger, and E. Dambrine. 2013. Tracing and modeling preferential flow in a forest soil: Potential impact on nutrient leaching. Geoderma 195–196:12–22. doi:10.1016/j.geoderma.2012.11.004

Vannoppen, W., M. Vanmaercke, S. De Baets, and J. Poesen. 2015. A review of the mechanical effects of plant roots on concentrated flow erosion rates. Earth Sci. Rev. 150:666–678. doi:10.1016/j.earscirev.2015.08.011

van Schaik, N.L.M.B. 2009. Spatial variability of infiltration patterns related to site characteristics in a semi-arid watershed. Catena 78:36–47. doi:10.1016/j.catena.2009.02.017

Wang, K., and R. Zhang. 2011. Heterogeneous soil water flow and macropores described with combined tracers of dye and iodine. J. Hydrol. 397:105–117. doi:10.1016/j.jhydrol.2010.11.037

Wang, Y., M. Shao, Z. Liu, and C. Zhang. 2015. Characteristics of dried soil layers under apple orchards of different ages and their applications in soil water managements on the Loess Plateau of China. Pedosphere 25:546–554. doi:10.1016/S1002-0160(15)30035-7

Williams, M.W., T.A. Erickson, and J.L. Petrzelka. 2010. Visualizing meltwater flow through snow at the centimetre-to-metre scale using a snow guillotine. Hydrol. Processes 24:2098–2110. doi:10.1002/hyp.7630

Wilson, G.V., and R.J. Luxmoore. 1988. Infiltration, macroporosity, and mesoporosity distributions on two forested watersheds. Soil Sci. Soc. Am. J. 52:329–335. doi:10.2136/sssaj1988.03615995005200020005x

Wu, G.L., Y. Liu, Z. Yang, Z. Cui, L. Deng, X.F. Chang, and Z.H. Shi. 2017. Root channels to indicate the increase in soil matrix water infiltration capacity of arid reclaimed mine soils. J. Hydrol. 546:133–139. doi:10.1016/j.jhydrol.2016.12.047

Yan, H., K. Li, H. Ding, C. Liao, X. Li, L. Yuan, and C. Li. 2011. Root morphological and proteomic responses to growth restriction in maize plants supplied with sufficient N. J. Plant Physiol. 168:1067–1075. doi:10.1016/j.jplph.2010.12.018

Yan, J., and W. Zhao. 2016. Characteristics of preferential flow during simulated rainfall events in an arid region of China. Environ. Earth Sci. 75:566. doi:10.1007/s12665-015-5101-4

Yang, L., W. Wei, L. Chena, W. Chen, and J. Wang. 2014. Response of temporal variation of soil moisture to vegetation restoration in semi-arid Loess Plateau, China. Catena 115:123–133. doi:10.1016/j.catena.2013.12.005

Yasuda, H., R. Berndtsson, H. Persson, A. Bahri, and K. Takuma. 2001. Characterizing preferential transport during flood irrigation of a heavy clay soil using the dye Vitasyn Blau. Geoderma 100:49–66. doi:10.1016/S0016-7061(00)00080-X

Zehe, E., T. Graeff, M. Morgner, A. Bauer, and A. Bronstert. 2010. Plot and field scale soil moisture dynamics and subsurface wetness control on runoff generation in a headwater in the ore mountains. Hydrol. Earth Syst. Sci. 14:873–889. doi:10.5194/hess-14-873-2010

Zhang, B., J.L. Tang, C. Gao, and H. Zepp. 2011. Subsurface lateral flow from hillslope and its contribution to nitrate loading in streams through an agricultural catchment during subtropical rainstorm events. Hydrol. Earth Syst. Sci. 15:3153–3170. doi:10.5194/hess-15-3153-2011

Zhang, J., and Z. Xu. 2016. Dye tracer infiltration technique to investigate macropore flow paths in Maka Mountain, Yunnan Province, China. J. Cent. South Univ. 23:2101–2109. doi:10.1007/s11771-016-3266-y

Zhang, Y., J. Niu, M. Zhang, Z. Xiao, and W. Zhu. 2016. Interaction between plant roots and soil water flow in response to preferential flow paths in northern China. Land Degrad. Dev. 28:648–663. doi:10.1002/ldr.2592

Zhang, Z.B., X. Peng, H. Zhou, H. Lin, and H. Sun. 2015. Characterizing preferential flow in cracked paddy soils using computed tomography and breakthrough curve. Soil Till. Res. 146(Part A):53–65. doi:10.1016/j.still.2014.05.016

Zhao, X.N., P.T. Wu, X.D. Gao, L. Tian, and H.C. Li. 2014. Changes of soil hydraulic properties under early-stage natural vegetation recovering on the Loess Plateau of China. Catena 113:386–391. doi:10.1016/j.catena.2013.08.023

Zhu, D., S. Hyun, J.J. Pignatello, and L.S. Lee. 2004. Evidence for π-π electron donor-acceptor interactions between π-donor aromatic compounds and π-acceptor sites in soil organic matter through pH effects on sorption. Environ. Sci. Technol. 38:4361–4368. doi:10.1021/es035379e